Journal of the Korean Nuclear Society
Volume 20, Number 2, June, 1988

Development of FURA Code and Application for Load Follow Operation

Young-Seob Park and Byong-Whi Lee
Korea Advanced Institute of Science and Technology
(Received February 24, 1988)

FURA 코드 개발과 부하 추종 운전에 대한 적용

박영섭 · 이병휘
한국과학기술원
(1988. 2. 24 접수)

Abstract

The FUel Rod Analysis(FURA) code is developed using two-dimensional finite element methods for axisymmetric and plane stress analysis of fuel rod. It predicts the thermal and mechanical behavior of fuel rod during normal and load follow operations. To evaluate the exact temperature distribution and the inner gas pressure, the radial deformation of pellet and clad, the fission gas release are considered over the full-length of fuel rod. The thermal element equation is derived using Galerkin's techniques. The displacement element equation is derived using the principle of virtual works. The mechanical analysis can accommodate various components of strain: elastic, plastic, creep and thermal strain as well as strain due to swelling, relocation and densification. The 4-node quadratic isoparametric elements are adopted, and the geometric model is confined to a half-pellet-height region with the assumption that pellet-pellet interaction is symmetrical. The pellet cracking and crack healing, pellet--cladding interaction are modelled. The Newton-Raphson iteration with an implicit algorithm is applied to perform the analysis of non-linear material behavior accurately and stably. The pellet and cladding model has been compared with both analytical solutions and experimental results. The observed and predicted results are in good agreement. The general behavior of fuel rod is calculated by axisymmetric system and the cladding behavior against radial crack is used by plane stress system. The sensitivity of strain aging of PWR fuel cladding tube due to load following is evaluated in terms of linear power, load cycle frequency and amplitude.

요 약

이차원의 유한요소법을 이용하여 axisymmetric과 R-θ system으로 나누어서 정상과 부하 추종 운전시에 핵연료 페렛트와 피복관의 열역학적 거동을 분석하기 위해서 FURA전산코드를 개발하였다. 온도분포와 내부압력을 정확히 계산하기 위해서 페렛트와 피복관의 변형과 핵분열의 기체방출을 전체핵연료봉길이로 고려하였다. 열역학적 평형방정식을 얻기 위해서 Galerkin's Technique과 가상일의 원리를 사용하였고 역학적 해석을 위해서 탄성-소성, 크리프 뿐만아니라 스웰링, 재배열, 고밀화 현상등을 고려하였다. 기하학적 모델에서는 4-결

점 요소와 페레트 길이의 1/2만을 택하였다. 비선형식을 안정하게 해석하기 위해서 음해법을 도입하여 뉴튼-랩손 반복법을 적용하였다. 이 코드의 검증은 해석해와 실험데이타로 비교하였다. 핵연료봉의 일반적인 거동은 axisymmetry system으로 계산하였고 균열된 페레트에 접촉하는 피복관의 거동은 R-θ system을 사용하였다. 부하추종에 의한 피복관의 변형 시효의 민감도는 출력율, 진동수, 진폭등으로 비교하였다.

Nomenclature

A area of element
B stran-displacement matrix
C creep matrix
E Young's modulus
E_c elastic modulus in completely cracked condition.
f creep function
|F| external force vector
h yield function
h_g heat transfer coefficient of gap gas
h_{gap} gap conductance
h_r heat transfer coefficient by radiation
h_s heat transfer coefficient at solid to solid contact spots
i iteration number, superscipt
j prinicipal direction, subscript
k thermal conductivity
[K] overall stiffness matrix in thermal and mechanical equation
$K_\theta T_{ij}$ terms of thermal element matrix equation for R-θ system
$K_z T_{ij}$ terms of thermal element matrix equation for R-Z system
n time step number
N_i interpolating function
n+ θ intermediate point between t_n and t_{n+1}
P_{fc} contact pressure between fuel and cladding
P_g gap gas pressure
P_ω coolant pressure
q''' heat genration rate per unit volume
R,r radial coordinate in global coordinate system
r_{ci} cladding inner radius
$R\theta_i$ terms of right-hand side column matrix in thermal matrix for R-θ system
RZ_i terms of right-hand side column matrix in thermal matrix for R-Z system
|Q| terms of right-hand side overall column matrix in thermal matrix
T temperature
|u| radial displacement vector
u_c radial displacement of clad
u_f radial displacement of fuel
U_f radial contact force of pellet
|v| axial and circumferential displacement vector
V volume of element
V_f axial contact force of pellet
Y plastic potential function
Z,z axial coordinate in global coordinate system

Greek letters

δ radial gap between fuel and cladding
δ_0 as-fabricated radial gap
δ_{fc} radial displacement of clad after contact
Δr_0 initial gap thickness
Δt time interval
$\{\varepsilon\}$ total strain vector
$\{\varepsilon^c\}$ creep strain vector
$\{\varepsilon^e\}$ elastic strain vector
$\{\varepsilon^o\}$ free expansion strain vector
$\{\varepsilon^p\}$ plastic strain vector
$\{\varepsilon^v\}$ creep strain rate vector
ε^H total creep strain
ε^p equivalent plastic strain
ε^{rel} initial relocation strain

θ tangential coordinate in global coordinate system
ϕ neutron flux
μ friction coefficient beween pellet and cladding
ν poisson's ratio
$\{\sigma\}$ stress vector
$\{\sigma'\}$ deviatoric stress vector
$\bar{\sigma}$ equivalent stress

1. Introduction

The experiences with the fuel rods of the water cooled reactor, in which uranium dioxide fuel pellets are clad with Zircaloy tubing, have shown that a sufficient severe power increase(ramp) can cause cladding failure, provided the burn-up is high enough. Another major cause of the cladding failure is PCI problem.

Any power increase produces an increased radial temperature gradient within the fuel pellets, and results in expansion of the pellets. The Zircaloy cladding is also subjected to the thermal stress, and becomes in contact with fuel pellets. Such phenomena, termed in pellet-cladding ineraction (PCI), usually brings about more complicated problems in analyzing the performance of the fuel rod system. It occurred that cracks are formed and grow due to the different radial thermal expansion. As fuel burns up, the hoop stress increases to a great extent around the contact point of the pellet and cladding. This hoop stress is responsible for the formation and propagation of cracks in the cladding.

In case of the load-following operation modes, the fuel cladding is subjected to high stresses, which change as a function of time. The changed high stresses affect the cladding failure.

There are many fuel performance codes for the analysis of the thermomechanical behavior of the fuel rod[1~8]. While the existing codes were considered on the one or two-dimensional approach, more accurate analysis may be required (based on three-dimension calculation) in the detailed evaluation of PCI problems associated with load-follow oriented studies, such as power ramping tests. However, three-dimension apporaches using FEM technique in fuel performance evaluation were rather complicated and limited to a theoretical level.

This work intends to give access to the problems occurring in the transient and local analysis of the fuel performance based on the quasi three-dimensional approaches, normally lateral plane (R-Θ system) and axisymmetric analysis (R-Z system).

The major purpose of this paper is to analyze the behavior of the local-part of the fuel rod in accordance with the power history including not only the steady-state case but also, the transient case including the load-following.

2. Theory

2.1. Code Structure

This code has two basic analysis capabilities i.e., lateral plane analysis (R-Θ system) and axisymmetric analysis (R-Z system). The former is mainly used in analayzing phenomena with axial variation such as hourglassing deformation of the pellet, ridging deformation of the clad, etc. The axisymmetric analysis is used in cricumferential variations such as clad stress and strain concentration caused by local interaction of cracked or relocated fuel pellets.

2.1.1. Geometrical models

The geometrical model used in this program is given in Fig. 1. For the R-Θ system, a fuel pellet is divided into the four concentric rings. The data of the thermal and mechanical properties are averaged over the width of each of these rings. For the R-Z system, a half of fuel pellet is divided into four axial segments. All the data averaged over the height of these segments are used in the calculations.

The region of half-pellet height is dealt with

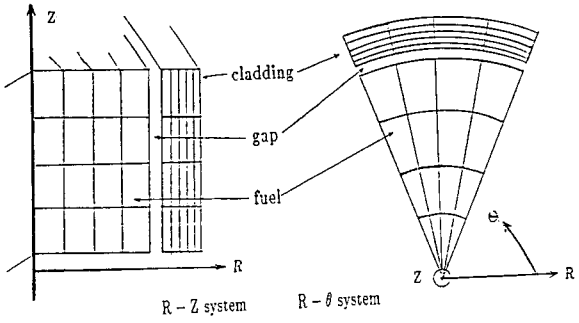

Fig. 1 Axisymmetric and Lateral Plane Analysis Sytem

assuming an axisymmetry and a plane-symmetry at the mid-plane of a fuel rod. A four-noded quadratic iso parametric element is used in building up the element stiffness equation. Also the stress, strain and material properties are assumed to be linearly varied in the element.

2.1.2. Code Description

A flow-chart of this program is shown in Fig. 2. The input includes data of geometrical variables, material properties, operational history, and initial values of temperature, stress, and strain. This program consists of two major calculation parts; the thermal analysis part and mechanical analysis part. In the thermal analysis part, the integral behavior of a whole fuel rod is analyzed and the temperature distribution and inner gas pressure are transfered to the mechanical analysis part where the local mechanical behavior is analyzed.

In the mechanical part, the boundary conditions at each interface node during the time step is initially assumed, based on the conditions in the previous step. Under this assumption, the preliminary calculations are made and first approximations of stresses and strains in the fuel and cladding are made. These first approximations for the creep strains are incorporated into the constitutive equations, which are combined with the equations of equilibrium relations and solved with the same boundary conditions. This solution yields a second approximation for the change in stress and strains in each integration point, which is then compared with the initial aprroximation. If agreement with specified limits is not made, iteration procedure is continued. After the convergence is achieved, the boundary coondition is updated and compared with the first assumption. If agreement is not made, iteration procedure is continued. There is another iteration loop to determine the contact condtion in each interface node couple whether in full bonding or in sliding. After completion of these iterations, if the calculated results show that the material state changes from open to contact or from contact to open, then the mechanical calculation is followed for residual time step until the end of time step is reached.

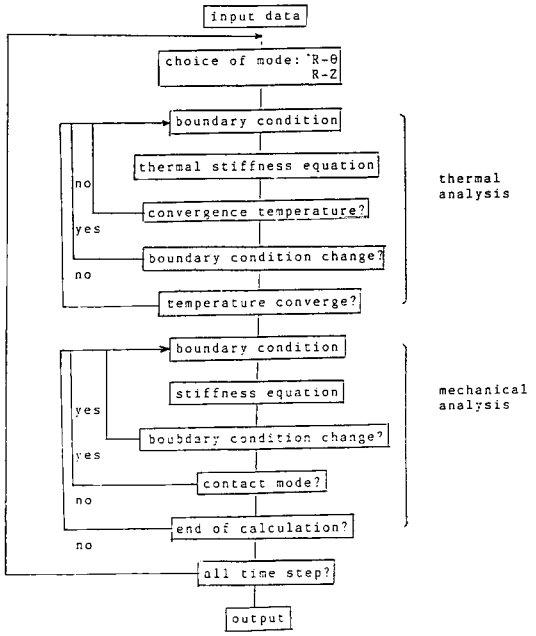

Fig. 2. Flow Chart of Program

2.2. Thermal Analysis Model

2.1.1. Heat Transfer Models

2.2.1.1. Pellet and Cladding Thermal Conductivity

The thermal conductivity of uranium dioixde is fairly well established, at least for low burn-up conditions. The thermal conductivity of UO_2 is expressed as a function of temperature and porosity.[9]

The thermal conductivity of Zircaloy is well established. Remaining uncertainties has only minor importance for the fuel rod behavior.

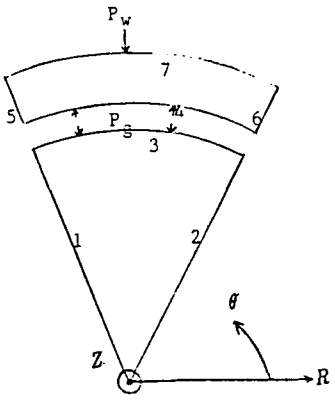

Fig. 3. Boundary Surfaces for R-θ System

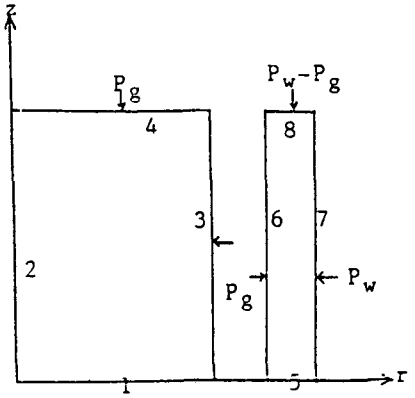

Fig. 4. Boundary Surfaces for R-Z System

Table 1. Restraint Conditionf for R-θ System.

Boundary surface number	R	θ	Restraint condition
1	F	R	|v| = |0|
2	F	R	|v| = |0|
3	F	F	
4	F	F	
5	F	R	|v| = |0|
6	F	R	|v| = |0|
7	F	F	

R: Restraint
F: Free

Table 2. Restraint Conditionf for R-Z System.

Boundary surface number	R	Z	Restraint condition
1	F	R	|v| = |0|
2	R	F	|u| = |0|
3	F	F	
4	F	F	
5	F	R	|v| = |0|
6	F	F	
7	F	F	
8	F	R	|v| = v_c

Values can be found in Ref. 9.

2.2.1.2. Gap Conductance

The heat transfer coefficient between fuel pellet and cladding is calculated by the modified Ross and Stoute model[10]. It is given as the sum of three components, heat transfer coefficients through gap gas, at solid to solid contact spots and by radiation as follows.

$$h_{gap} = h_g + h_s + h_r \quad (1)$$

2.2.1.3. Temperature Distribution in the Pellet and Cladding

To obtain temperature distribution in fuel rod, two-diemnsional heat conduction euqation[13] is used.

For R-Θ system,

$$\frac{\partial}{\partial r}\left[kr\frac{\partial T}{\partial r}\right]+\frac{1}{r}\frac{\partial}{\partial \theta}\left[k\frac{\partial T}{\partial \theta}\right]+rq'''=0 \quad (2)$$

and for R-Z system,

$$\frac{\partial}{\partial r}\left[kr\frac{\partial T}{\partial r}\right]+\frac{1}{r}\frac{\partial}{\partial z}\left[k\frac{\partial T}{\partial z}\right]+rq'''=0 \quad (3)$$

2.2.2. Pellet-Cladding Gap Change and Contact pressure

One troublesome area in the analysis is the estimation of gap change due to the following phenomena;

(1) Fuel thermal expansion: The fuel thermal expansion contributes strongly to peak hoop stresses and consequently also PCI failures. The fuel thermal expansion is given as a function of temperature[9].

(2) Fuel relocation: the cylindircal fuel pellets

crack due to the combined effect of thermal stresses. The cracks run predominantly radially from the center to outwards when seen from the end of pellet, and transverse across the pellet when viewed from the side. The fragments of cracked fuel are relocated outward to reduce a certain fraction of the gap.

(3) Fuel swelling and densification: these process changes the dimensions of the fuel pellets under irradiation. The densification cause the pellet to shrink. The rate of densification is largest at the start of irradiation and decrease with burn-up and eventually stops. An empirical expression for the change of porosity volume is a function of burnup[11]. The swelling is caused by the fissioning of heavy uranium atoms producting fission products with lower density. It is thus a process aproximately proportional to burn-up. Some of calculations, it is generally easy to handle the sole effect of the solid fission products while swelling due to gaseous fission products is much more complex. The swelling rate due to solid fission product is given in Ref.11 and that due to the retension of gaseous fission product is given as a function of fuel temperature and fission numbers.

(4) Cladding thermal expansion: the clad thermal expansion contributed very little to the variation in the peak clad stress. The cladding thermal expansion is given as a function of temperature.[9]

(5) Cladding Creep deformation: the cladding creep helps to reduce the stress during and after power ramps. The radial displacement of the cladding by creep is given as a function of burnup, inner and outer pressures.[4].

The radius of fuel pellet is varied with phenomena such as thermal expansion, relocation, densification, and gaseous and solid swelling. And the cladding radial displacement is also varied with thermal expansion, elastic and creep deformations. When gap change occurs by these phenomena, the gap is given as follows:

$$\delta = \delta_o + u_c - u_f \tag{4}$$

The cladding radial displacement after contact is given by

$$\delta_{fc} = -(\delta_o + u_c - u_f) \tag{5}$$

The contact pressure between fuel and cladding is calculated by

$$P_{fc} = \frac{\delta_{fc} E_c \Delta r_c}{r^2_{ci}} \tag{6}$$

2.2.3. Derivation of the Thermal Element Equation

Galerkin's technique applied to this equation yields for node i of the element; for R-Θ system

$$\int_A \left\{ \frac{\partial}{\partial r}\left[kr \frac{\partial T}{\partial r} \right] + \frac{1}{r} \frac{\partial}{\partial \theta}\left[k \frac{\partial T}{\partial \theta} \right] + rq''' \right\} \cdot N_i r dr d\theta = 0 \tag{7}$$

and for R-Z system

$$\int_A \left\{ \frac{\partial}{\partial r}\left[kr \frac{\partial T}{\partial r} \right] + \frac{1}{r} \frac{\partial}{\partial z}\left[k \frac{\partial T}{\partial z} \right] + rq''' \right\} \cdot N_i r dr d\theta = 0 \tag{8}$$

where A designates integration over the whole area of the element and N_i are the interpolating functions. Applying the Green's theorem described in Eqs. (7) and (8), and to the interpolating function[12], the element equation at node i is given as;

for R-Θ system

$$\sum_{j=1}^{4} K_\theta T_{ij} T_j = R\theta_i \tag{9}$$

and for R-Z system

$$\sum_{j=1}^{4} K_z T_{ij} T_j = RZ_i \tag{10}$$

Each term in Eqs. (9) and (10) is presented in ref.22. Equation (9) and (10) are applicable to a single node within a single element. In order to produce an overall matrix equation, the process of assemblage of the element equation is needed and gives the following overall matrix equation:

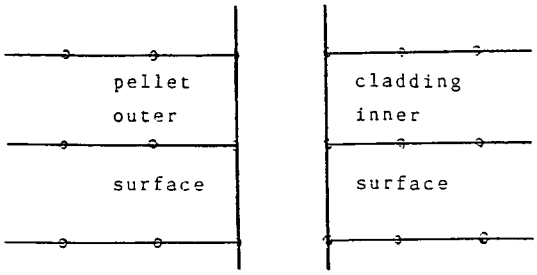

Fig. 5. Node Couples on the Pellet-Cladding Interface

$$[K]\{T\} = \{Q\} \tag{11}$$

where [K] represents the overall stiffness matrix and the right hand side column vector, $\{Q\}$, is value which were calculated from the previous iteration step.

2.3. Mechanical Behavior Analysis Model

2.3.1. General Relations

In the derviation of the displacement equation, the principle of virtual displacement[14] is adopted. The force-diplacement equilibrium equation in the form of successive iterations is given as

$$\int_v B^T \{\sigma^i_{n+1}\}\, dV + \int_v B^T \{\sigma^{i+1}_{n+1}\}\, dV - \{F_{n+1}\} = 0 \tag{12}$$

The problems considered here includes the non-linear material behaviors such as creep, plasticity, and fuel cracking. Taking into account these non-linear problems, the constitutive relations are formulated by the incremental approach.

In general the strain vector can be expressed as the sum of four components; elastic, creep, plastic and free expansion.

$$\{\Delta\varepsilon_{n+1}\} = \{\Delta\varepsilon^e_{n+1}\} + \{\Delta\varepsilon^c_{n+1}\} + \{\Delta\varepsilon^p_{n+1}\} + \{\Delta\varepsilon^o_{n+1}\} \tag{13}$$

where

$\{\Delta\varepsilon_{n+1}\}$ = *incremental total strain vector*

$\{\Delta\varepsilon^e_{n+1}\}$ = *incremental elastic strain vector*

$\{\Delta\varepsilon^p_{n+1}\}$ = *incremental plastic strain vector*

$\{\Delta\varepsilon^o_{n+1}\}$ = *incremental free expansion strain vector*

$\{\Delta\varepsilon^c_{n+1}\}$ = *incremental creep strain vector*

Table 3. The Judging Criteria for the Contact Node Couple

Contact condition Before	After	Judging criteria
	open	($\delta > 0$)
open	contact	($\delta > 0$)
	open	($U_f > 0$)
full	full bonding	$U_f < 0$, $\lvert V_f \rvert < \mu \lvert U_f \rvert$
bonding	sliding	$U_f < 0$, $\lvert V_f \rvert < \mu \lvert U_f \rvert$
	open	$U_f > 0$
sliding	full bonding	$U_f < 0$, $\lvert V_f \rvert < \mu \lvert U_f \rvert$
	sliding	$U_f < 0$, $\lvert V_f \rvert > \mu \lvert U_f \rvert$

U_f: radial contact force of pellet
V_f axial and circumferential contact forece of pellet
μ: friction coefficient between pellet and clad

relationship are presented in refernce 14 and 15.

2.3.2. Creep

The creep theory is used in the strain hardening theory. The uniaxial creep strain rate is usually defined as a function of stress, total creep stain, temperature, and fast neutron flux, namely

$$\{\dot{\varepsilon}^c\} = f(\{\sigma\}, \varepsilon^H, T, \phi) \tag{14}$$

Using a creep flow rule as in plasticity theory, Eq.(14) can be extended into multiaxial state as follows:

$$\{\dot{\varepsilon}^c\} = \frac{3}{2}\frac{f}{\sigma}\{\sigma'\} \tag{15}$$

The most common method of creep analysis in the finite element method is the initial strain method, in which the creep strains are expressed in an explicit form. The drawback of this approach is the fact that the time interval must be very small if the creep rate is high [15], because the solution becomes numberically unstable. An implicit algorithm has been adopted to obtain the stable solution if the power is high.

The incremental creep strains $\{\Delta\varepsilon^c_{n+1}\} =$ is assumed to be written as

$$\{\Delta\varepsilon^c_{n+1}\} = \Delta t_{n+1}\{\dot{\varepsilon}^c_{n+\theta}\} \tag{16}$$

The following relations hold at that time.

$$\{\sigma^{i+1}_{(n+\theta)}\} = \{\sigma^i_{n+\theta}\} + \theta\{d\sigma^{i+1}_{(n+\theta)}\} \tag{17}$$

$$\Delta \varepsilon^{H,i+1}_{(n+1)} = \varepsilon^{H,i+1}_{(n+\theta)} \Delta t_{n+1} \quad (18)$$

$$\varepsilon^{H,i+1}_{(n+1)} = \varepsilon^{H,i}_{(n+1)} + \theta d\varepsilon^{H,i+1}_{(n+1)} \quad (19)$$

Expanding Eq.(16) and (19) in a Taylor series of the first order aobut $\{\sigma^{i+1}_{(n+\theta)}\}$ and $d\varepsilon^{H,i+1}_{(n+1)}$ and rearranging the two equations for eliminating $d\varepsilon^{H,i+1}_{(n+1)}$, we have finally

$$\{\Delta \varepsilon^{i+1}_{(n+1)}\} = \{\Delta \varepsilon^{i}_{n+1}\} + C^{c,i}_{(n+\theta)} \{d\sigma^{i+1}_{(n+1)}\} \quad (20)$$

The detailed expression for $C^{c,i}_{(n+\theta)}$ is in Ref.4.

2.3.3. Plasticity

The yield criterion can be, in general, expressed as

$$h(\{\sigma\}) = Y(\bar{\varepsilon}^{p}, T) \quad (21)$$

where $\bar{\varepsilon}^{p}$ is the hardening parameter which is defined as the effective plastic strain, and T is the temperature. The plastic strain increments must obey the following flow rule.[17]

$$\{\Delta \varepsilon^{p}_{n+1}\} = \Delta \varepsilon^{p}_{n+1} \left\{\frac{\partial h}{\partial \sigma}\right\}_{n+\theta} \quad (22)$$

Writting Eqs.(21) and (22) in the form of iteration.

$$h(\{\sigma_n\} + \{\Delta \varepsilon^{i+1}_{(n+1)}\}) = Y(\bar{\varepsilon}^{p}_{n} + \Delta \bar{\varepsilon}^{p,i+1}_{(n+1)}, T_n + \Delta T_{n+1}) \quad (23)$$

$$\{\Delta \varepsilon^{p,i+1}_{(n+1)}\} = \Delta \bar{\varepsilon}^{p,i+1}_{(n+1)} \left\{\frac{\partial h}{\partial \sigma}\right\}^{i}_{n+\theta} \quad (24)$$

Expanding Eq.(23) in a Taylor series of the first order about $\Delta \varepsilon^{p,i+1}_{(n+1)}$ and ΔT_{n+1}, the expression for $\Delta \bar{\varepsilon}^{p,n+1}_{(n+1)}$ can be derived [4].
$d\sigma^{i+1}_{(n+1)}$ is obtained considering the incremental creep and plastic strain vector. Substituting this into Eq.(12) and rearranging the equation, we have the following stiffness equation to be solved for the displacements $\{\Delta u^{i+1}_{(n+1)}\}$.

$$[K_{n+\theta}]\{\Delta u^{i+1}_{(n+1)}\} = \{\Delta \bar{F}^{i}_{n+1}\} \quad (25)$$

where, $[K_{n+\theta}]$ and $\{\Delta \bar{F}^{i}_{n+1}\}$ are the finite element stiffness matrix and the force vector. The finite element stiffness matrix and the force vector are presented in detail.[4]

The above stiffness matrix and force vector are computed by using the Gaussian formula of numerical integration with 3×3 integration points.[18]

2.3.4. Effect of Pellet Cracking

Fuel cracks are usually observed to occur on the principal planes, which are perpendicular to radial, axial, and circumferential direction, and are therefore associated with the principal stresses.

The crack is viewed as a mechanism which changes the material behavior from isotropic to orthotropic. The elastic modulus for fuel under cracking and crack healing is given:

$$E_j = -\frac{\varepsilon^{e}_{(m)}}{\varepsilon^{rel}_{j}}(E - E_c) + E_c, \text{ if } -\varepsilon^{rel}_{j} < \varepsilon^{e}_{2j} < 0 \quad (26)$$

$$E_j = E_c, \text{ if } \varepsilon^{e}_{j} > 0 \quad (27)$$

$$E_j = E, \text{ if } \varepsilon^{e}_{j} < -\varepsilon^{r}_{j}el \quad (28)$$

where E_c *is the very small value, j is the directional suffix and* ε^{rel}_{j} is the initial strain due to relocation.

3. Application

3.1. Code Validation

The program validation of code is presented in order to give its confidence.

To validate the computer code FURA, the analytical solutions available are compared with the numerical results simulated using this code. Experimental data are also used in the case that no analytical solutions exits. The validation for the thermal model is made using the geometry model given in Fig. 6, and the necessary material properties listed in Table 4. Fig. 7 shows that comparing the analytical solutions with the calculated results those are in a good agreement in each discrete point of our concerns.

For the mechanical model validation, the behavior of the displacement and hoop stress are dealt with using the geometrical model in Fig. 8,

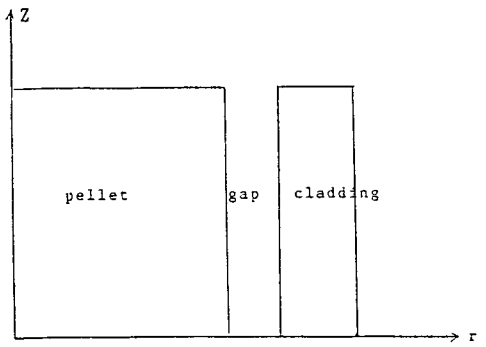

Fig. 6. Geometry for Validation for the Thermal Part

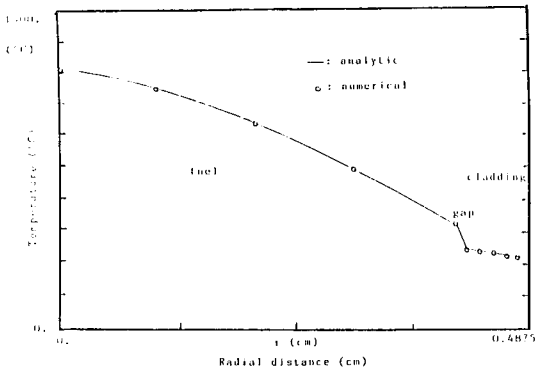

Fig. 7. Temperature Distribution in Fuel and Cladding

Table 5. Material Properties and necessary quantities.

Young's modulus	1.9×10^5 MPa
Poisson's ratio	0.316
Yield stress	$50\sqrt{3}$ MPa
Strain harden parameter	0.0
Inner radius	0.2 cm
Outer radius	0.5 cm
Outer pressure	10 MPa

that is the cylinderical model with a concentric circular hole. Their material properties are listed in Table 5. The analytical solutions for the radial displacement of the surface due to hoop stress with a variable pressure was given by Ref.20. The solutions are compared with the numerical solutions of the program, considering the variation of the radial displacement with increasing the inner pressure. Fig. 9 shows a good agreement between

Table 4. Material Properties and Necessary Quantities.

pellet radius	0.41 cm
diameter gap	0.08 cm
average coolant temperature	305°C
heat transfer coefficient	3.36 W/cm^2.°C
gap conductance	1.0 W/cm^2.°C
conductivity fuel	0.0268 W/cm.K
cladding	0.1338 W/cm.K
heat generation rate	455 W/cm^3

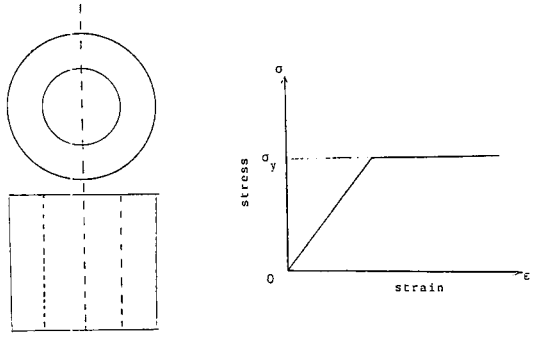

Fig. 8. Geometry for Stress and Displacement

them. And we know that the low internal pressure does not induce plastic deformation but high internal pressure in the inner region. This value of internal pressure in 63.2 MPa. Such characteristics as the plastic deformation in the program output and analytical solutions are plotted in Fig. 10 and Fig. 11. Fig. 10 shows the distribution of the hoop stress in the elastic region and Fig. 11 in the case both elastic and plastic region.

In the thermo mechanical analysis, the geometry model and their involved material properties are shown in Fig. 12, and Table 6 repsectively. Comparisons between the analytical[21] and numerical solutions for the radial displacement are plotted in Fig. 13, and the distribution of all stress components in Fig. 14. Since the size of the finite elements is rather larger, it is natural that slight relative errors should occur between the numerical and analytical solutions.

The creep down of cladding as burn-up increases is compared with the experimental data[22]

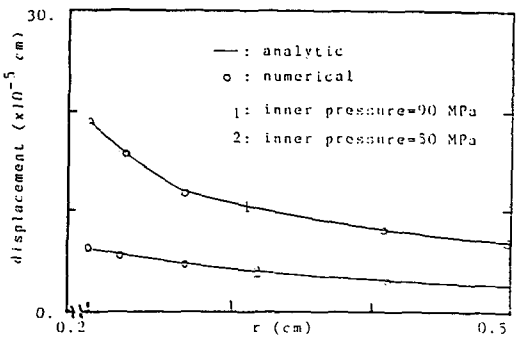

Fig. 9. Incremental Displacement Distribution

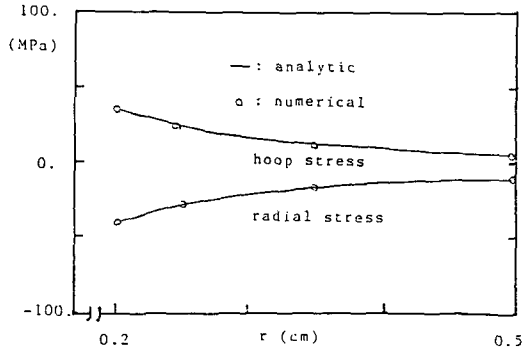

Fig. 10. Strees Distribution in Elastic Region

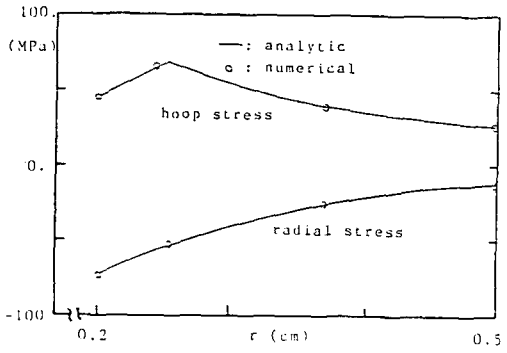

Fig. 11. Stress Distribution in Elastic-Plastic Region

Table 6. Material Properties and Necessary Quantities.

Inner radius	0.2 cm
Outer radius	0.5 cm
Young's modulus	1.9×10^5 MPa
Poisson's ratio	0.316
Inner pressure	5 MPa
Outer pressure	15 Mpa
Thermal expansion coefficient	0.05×10^{-4}
Temperature of outer surface	100°C
Thermal conductivity	0.14 W/cm.°K
Heat generation rate	120 W/cm^3

in Fig. 15. The computation results are slightly low values.

3.2. Thermal Analysis

As power increases, the gap conductance increases with decreasing gap and decreases due to released fission gas. In that model, the heat transfer due to radiation is very small and that through solid and solid spots is increasing when the contact occurs. The numerical value of the gap conductance increases as a whole. Vitanza empirical model[4] is used as a fission gas release model, which is described by a function of the fuel temperature and burn-up. Inner gas pressure is derived from ideal-gas law considering thermal expansion of fuel, fuel relocation, fuel densification, fuel swelling, clad creep deformation and values of initial and released fission gas. The convective heat transfer coefficient for the forced convection can be calculated using the Dittus-Boelter

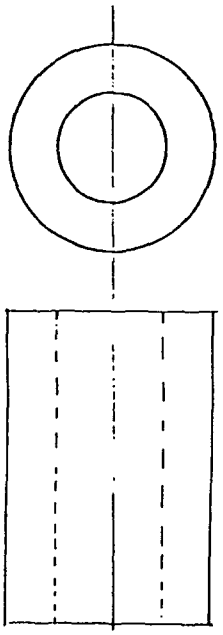

Fig. 12. The geometry of a Cylinder With a Concentric Circular Hole

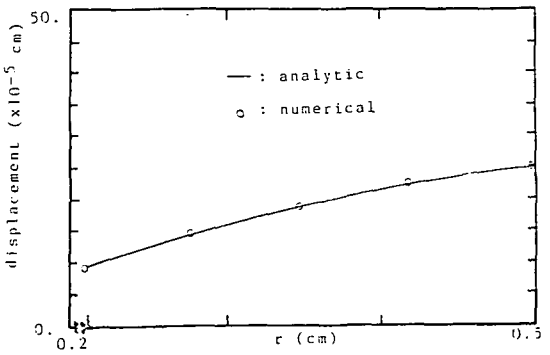

Fig. 13. Radial Displacement Distribution

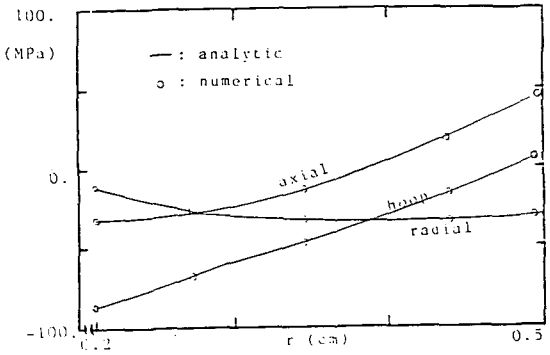

Fig. 14. Distribution of Normal Stress Components

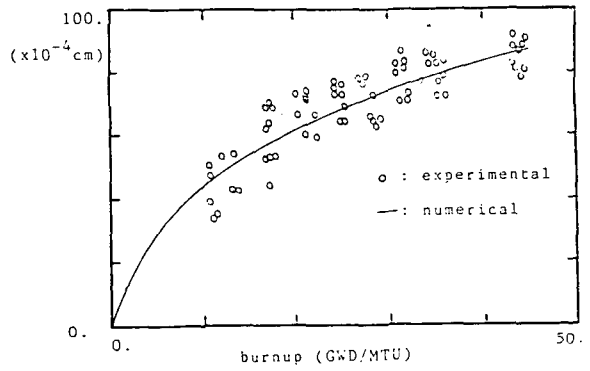

Fig. 15. Cree-dowpn vs. Burnup

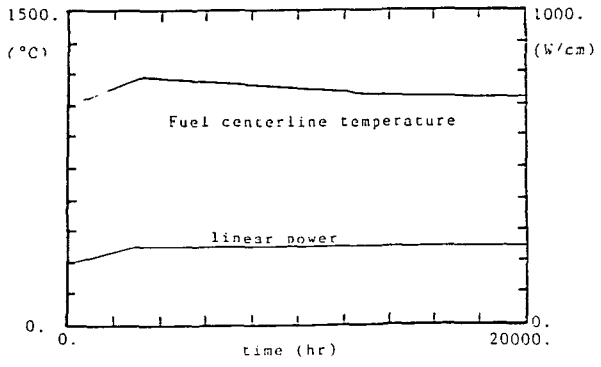

Fig. 16. Fuel Centerline Temperature with the Lapse Time

correlation.[19] Table 8 shows the related fuel geometry and various coolant conditions. The coolant temperature is considered as constant for one fuel pellet.

As constant power operation is proceeding, the fuel centerline temperature decreases because of decreased gap conductance. This result is shown in Fig. 16.

Table 8. Properties of Coolant

coolant thermal conductivity	0.0054 W/cm.°C
equivalent hydraulic diameter	1.18 cm
coolant velocity	4.33 m/sec
coolant density	0.716 g/cm^3
visocisity of coolant	0.0904 g/m.sec
Prandtl number	0.9239
specific heat	4.187 J/kg.°C
average coolant temperature	305°C

3.3. Mechanical Behavior Analysis of a Non-Cracked Fuel pellet and Cladding

A fuel pellet deforms by various factors, such as thermal expansion, swelling, densification, etc. The cladding also deforms by thermal expansion, creep, etc. The dominant one among the various factors is said to be the effect of thermal loading.

The temperature distribution and inner gas ressure calculated in the thermal part of the program is directly used in the calculation of the mechanical properties and the distribution of the stress. The analysis is applied to a specified region of the half-pellet height, which is considered as a minimum scale of the geometrical model. Though the boundary condition of surface is previously listed in Table 3, we assume the spring force at the upper part of the pellet is 3.26 MPa without considering the effect of te pellet-pellet interaction.

The stresses are calculated for the power level of 250 W/cm. In this calculation the pressure of the coolant is assumed to be a constant value,

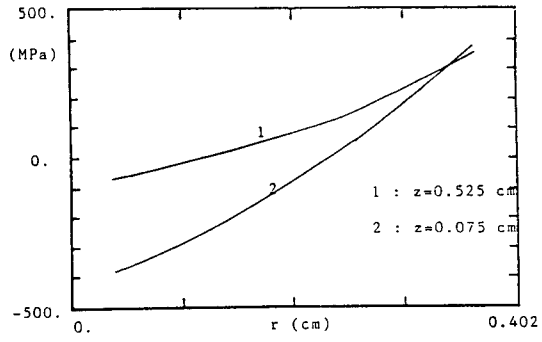

Fig. 17. The Hoop Strees Distribution of Pellet Non-Crack

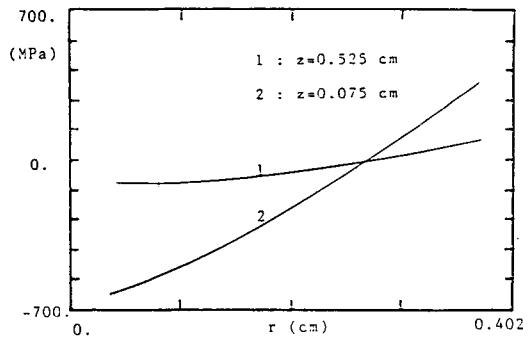

Fig. 18. The Axial Stress Distributin of Pellet with Non-Crack

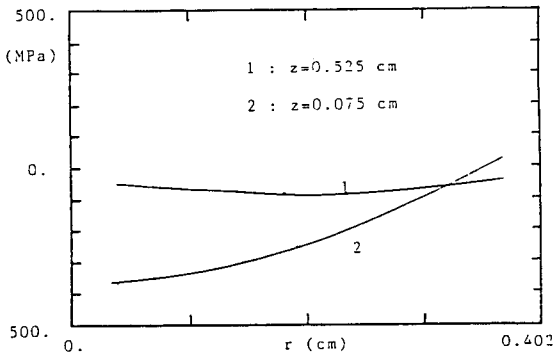

Fig. 19. The radial Stress Distribution of Pellet with Non-Crack

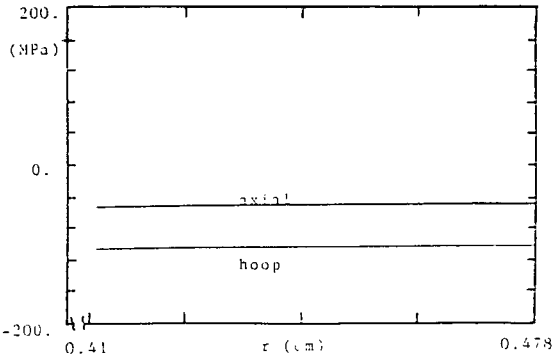

Fig. 20. The Hoop and Axial Stresses of Cladding with Non-Crack.

15.382 MPa. The three normal stress components of the fuel pellet and clad are plotted in Fig. 17 through Fig. 20. In ths case when the pellet cracking is not considered, the plastic deformation proceeds from center of the fuel of power exceeds more than certain limits. In the clad, however, the plastic deformation does not occur before the contact between pellet and clad. For fuel pellet, the radial stress is compressive, the hoop and axial stress components are compressive in the central region of the pellet and tensile in the outer region, because of the dominant thermal stress in the centeral region.

As reactor operation is proceeding, the stresses of pellet rather decrease and those of cladding increase because of temperature variation with time. But these variation quantities are small.

3.4. Mechanical Behavior Analysis of a Cracked Pellet and Cladding

At the beginning of the reactor operation, the differential thermal expansion in accordance with radial region of fuel pellet induces thermal stress and initiates pellet crack. The crack model is mentioned as described previously. We assumed that the formation of a micro-crack in one of the three principal direction occurs when the elastic strain in that direction becomes a tensile value. Therefore, during initial power ramp escalation, the pellet micro-crack nucleate both axially and radially in outer region of pellet.

As the ractor operation proceeds, the fuel pellet bulges by thermal expansion and fuel swelling, and the clad contracts by creep-down. As a result, the cracked pellet and clad makes contact. The

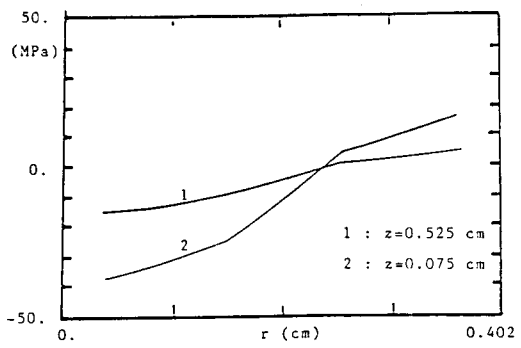

Fig. 21. The Axial Stress Distribution of Pellet with Crack

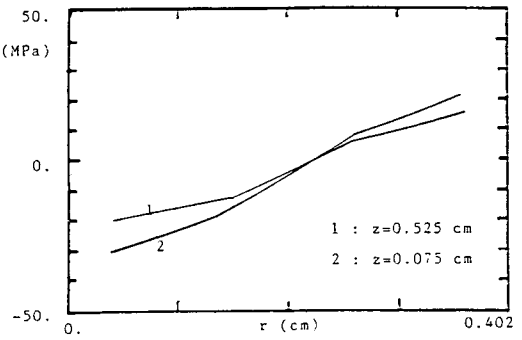

Fig. 22. The Hoop Stress Distribution of Pellet with Crack

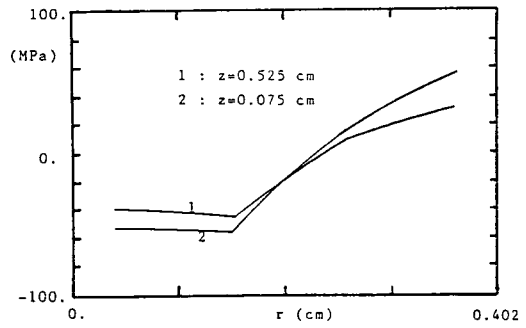

Fig. 23. The Hoop Stress Distribution of Pellet with Hard Contact

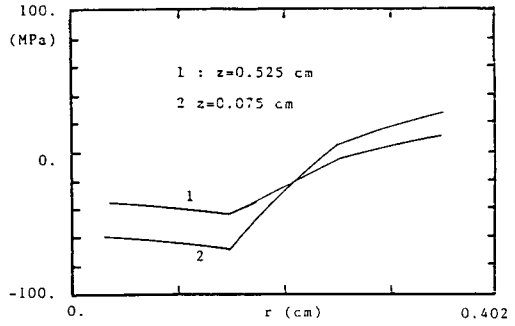

Fig. 24. The Axial Stress Distribution of Pellet with Hard Contact

forces resutls in clad deformations and stresses at contact points. Estimates of these induced clad stresses are important becuase those have been postulated to be a major contributor to fuel rod failures.

For no contact, at the linear power level of 250 W/cm and 2500 hr operation time, the normal stresses of the pellet fragments is plotted in Fig. 21 and 22. Before the cracked pellet and clad contact, the fuel pellet and clad does not deform plasticaly. As shown in Fig. 21 and Fig. 22, the stresses of the outer region in fuel pellet is low values becuase of a cracked pellet. If the linear power is between 200 W/cm and 300 W/cm, the contact occurs when the operating time is between 800 days and 1200 days. As time passes, the contact forec increases.

For hard contact, at the linear power of 250 W/cm, the normal stresses of the fuel pellet are plotted in Fig. 23 and 24. The yield region of the fuel pellet is inner region, while the outer region of fuel pellet does not deform plastically becuase of cracked portion of the fuel pellet. The clad deforms plastically, the hoop stress of cladding is positive because the sum of inner pressure and contact forces is greater than system pressures. The hoop stress distribution of cladding is shown in Fig. 25. In order to analyze the detailed clad behavior when the radial crack of pellet fragment occurs under contact with cladding, For R-Θ system, a simple model is considered as shown Fig. 26[22]. When the linear power is 400 W/cm, the normal stress distirbutions of the cladding opposite to the crack is plotted in Fig. 27. By the contact force, the hoop stresses are highly tensile at the inner surface. The stress concentration of cladding

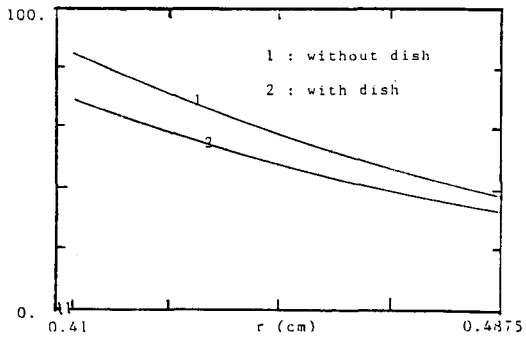

Fig. 25. The Hoop Stress Distribution of the Cladding with Hard Contact

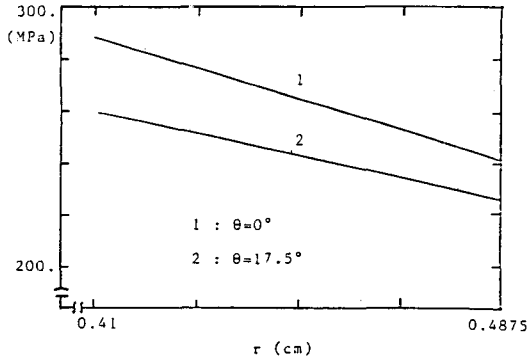

Fig. 27. The Hoop Stress Distribution of Clad Opposite to Crack

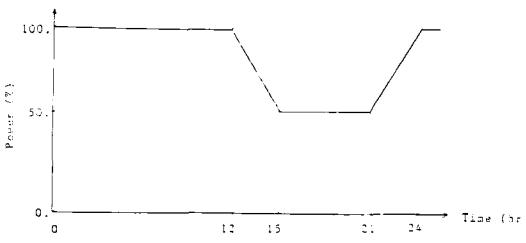

Fig. 29. The Model of Load-follow Operation

around pellet crack is showed in Fig. 28. In Fig. 28, the finite element of clad is coarse and these values are very rough.

3.5. Application to Load Follow Operation

The load follow operations are inserted during rod lifetime, and the model is shown as Fig. 29. The only noticeable effect of load following is an increase in clad hoop stress. If the pellet-clad gap is closed at the time of load following, the hoop

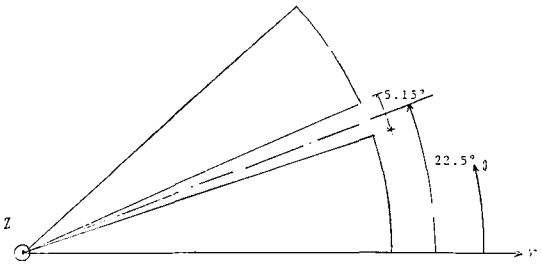

Fig. 26. Geometry Model for Cracked Pellet Fragment

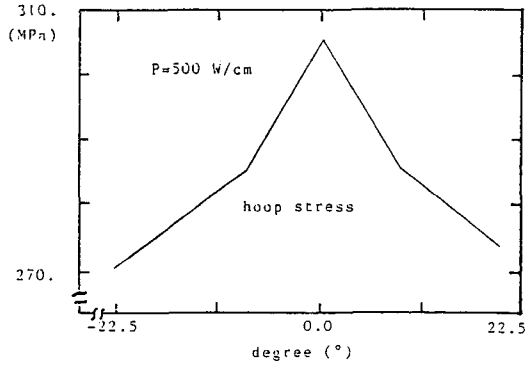

Fig. 28. The Stress Concentration of Cladding Around Pellet Crack

stress reaches moderately high tensile values, thus increasing the PCI failutre probability. When the pellet-clad contact does not occure, the load-follow stresses are equal to the initial stresses. At somewhat higher burn-up, the pellet-clad contact occurs during load follow operation, giving slightly higher stresses for this mode operation. At high burnups, around 40 GWD/MT, the pellet is in contact with the clad even during base load operation and load follow operation increases the clad hoop stresses by about 180 Pa. After the pellet-clad contact occure, the incremental hoop stress of clad is shown in Fig. 30 up to 40 daily load cycling is operated. At initial 30 daily load cycling, the loop stress of clad increases but the hoop stress of clad converges at the latter load cycling. When the reactor is operating at various linear power level, the incremental hoop stress of clad is a little higher in low power level than in high power level for the case of one daily cycle. But the number of daily cycle to the satuation of

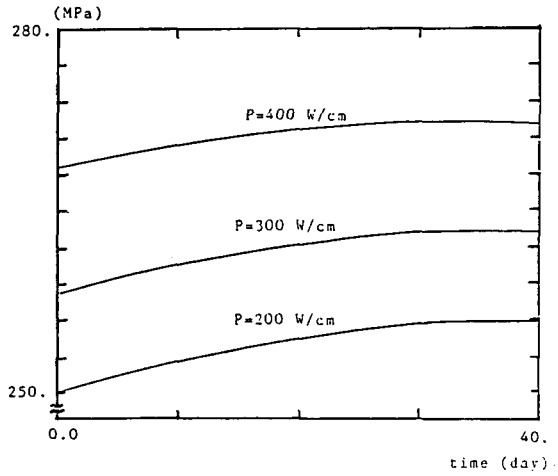

Fig. 30. Incremental Quantities of Hoop Stress During Load-Following

hoop stress is nearly constant. For the upper constant power level of daily cycle and various lower power level, 30%, 50% and 70% of full power, the amplitude of cycle does not rarely affect the incremental hoop stress of clad. The reason is that the pellet and clad does not contact at lower operation. During 30 daily cycling operation after PCI was initiated, the hoop strain and permanent hoop strain of clad at the pellet end is plotted in Fig. 31. As shown in Fig. 31, the incremental permenent hoop strain of clad per one cycle slowly decreases during load follow operation. The interval of hoop strain of clad between full power level and 50% power level is equal, becuase this value represents elastic hoop strain.

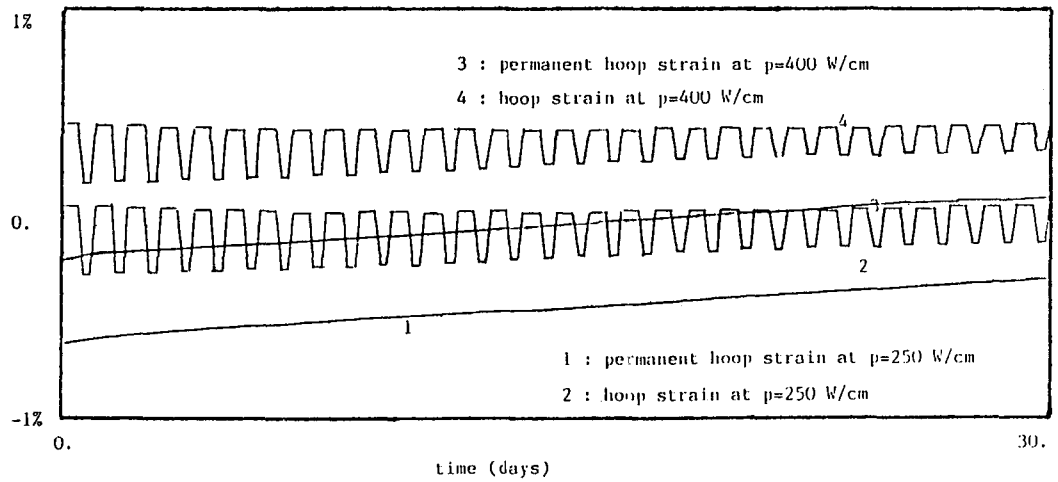

Fig. 31. The Hoop and Permanent Hoop Strain of Cladding (Burnup=40 GWD/MTU)

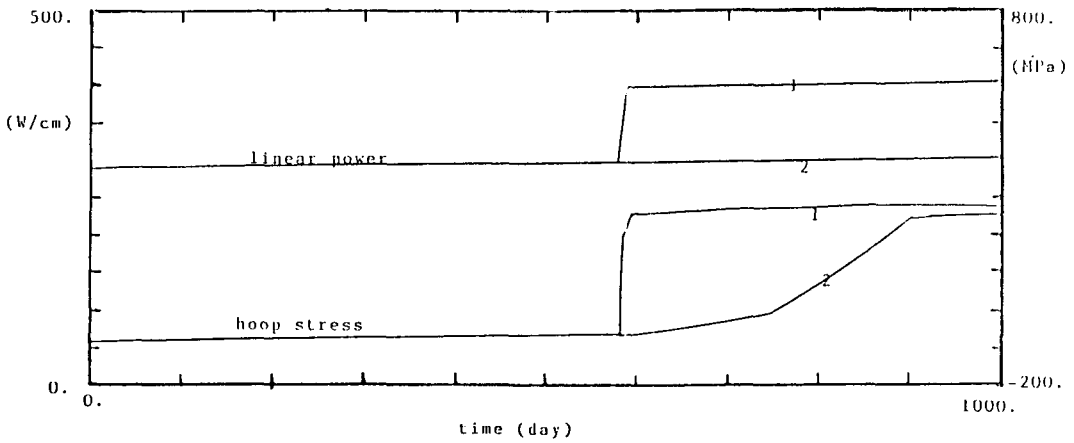

Fig. 32. Power and Hoop Stress Variation During Operation

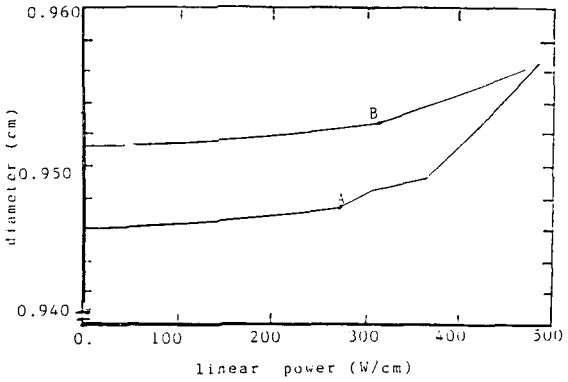

Fig. 33. The Cladding Outside Diameter During the Power Ramping Cycle

From initial operation to 1000days, the hoop stress of cladding versus linear power is plotted in Fig. 32. As shown in Fig. 32, the hoop stress is negative before PCI occurs and tensile after PCI. After contact is established, the cladding outside diameter is changed during the power ramping cycling. The difference of cladding diameter between before ramping cycle and after ramping cycling is the plastic deformation quantities. The cladding outside diameter during the power ramping cycle is plotted in Fig. 33. At point A, the contact between pellet and clad is initiated, at point B, the condition is open state.

4. Conclusions

The validation of program is performed in comparison with analytic solutions and experimental data. The predicted results are in good agreement with the analytical solutions and experimental data. As a result suggested that:

1) As the constant power operation is proceeding, the fuel centerline temperature is slowly decreased because of the increased gap conductance.

2) After contact is established, the hoop stress of cladding due to contact forces is positive and affect the cladding failure.

3) In the parts of the cladding which is opposite to the radial crack, the hoop stress of cladding nearly exceed the ultimate tensile strenth for 500 W/ cm of linear power. Therefore, in the value above of 500 W/cm linear power, the failure of clad is initiated.

4) At high burnups, one load follow cycle increases the clad hoop stress by about 180 Pa. The cladding hoop stress constantly increases during first 30 daily cycling operation, and then is nearly constant. The incremental hoop stress of clad for daily cycle is affected by liner power, but the total number of daily cycle to the saturation of hoop stress is hardly affected by linear power. The amplitude of cycle is negligible for the hoop stress of clad at constant upper power level.

5) During load follow operation, the incremental permanent hoop strains of cladding gradually decreases.

To precisely predict the hoop stress of clad against radial pellet crack, a portion around radial pellet crack is divided minute finite element. Also the pellet-pellet interaction and chamfer of pellet are needed for exact solutions.

References

1. harriague S., Coroll G. and Savino E. J., BACO, a computer code for simulating a reactor fuel rod performance, Nucl. Eng. Des. 56(1980) 91-103.
2. Vliet J. Van. and Meulemeester E. de., General description and organization of COMETHE III-J, Nucl. Eng. Des. 56(1980) 71-76.
3. Notley M. J. F., ELISIM: A computer code for predicting the performance of nuclear fuel elements, Nucl. Technol. 44(1979) 44-450
4. Kinoshita M. Ichikawa M. etal., FEMAXI-III: A Computer Code for Analysis of Thermal and Mechanical Behavior of Fuel Rods, JAERI, 1985.
5. Nuno H., ogawa S. and Kobayashi H., The "THERMOST" for analysing thermostructural behavior of LWR fuel rod under PCI condition. IAEA Specialists Meeting on Fuel Element Performance Computer Modelling, Preston, UK, 14-19 March 1982, p. 251.
6. Nuno H. eta., FROST code for predicting fuel rod performance, IAEA Specialists Meeting, Blackpool UK, March 1978.
7. Berna G. A., Bohn M. P., Rausch W. N., Williford

R. E. and Lanning D. D. FRAPCON-2; A computer code for the claculation of steady state thermal--mechanical behavior of oxide fuel rods, NUREG/CR-1845(1980) 295p.

8. Lassmann, K., URANUS A computer programme for the thermal and mechanical analysis of fuel rods in a nuclear reactor, Nucl. Eng. Des. 45(1980) 151-161.
9. MATPRO-11, A handbook of materials properties for use in the analysis of Light Water Reactor fuel rod behavior, NUREG/CR-0497, 1981.
10. A. M. Ross and R. L. Stoute, Heat Transfer Coefficient between UO_2 and Zricaloy-2, CRFD-1075; ACEL-1552(1962).
11. D. G. franclin et al., Low Temperature Swelling and Densification Properties of LWR Fuels, J. of Nucl. Mat., 125, 96-103(1984)
12. J. J. Chung, Finite Element Analysis in Fluids and Heat Transfer, University of Alabama Press, 1981.
13. J. P. Holman, Heat Transfer, 5th ed., McGraw-Hill, 1981.
14. O. C. Zienkiewca, The Finite Element Method, 3rd ed., 21-500, McGraw-Hill Book Company, U. K. (1977)
15. K. J. Bathe, Finite Element Procedures in Engineering Analysis, Prentice-Hall, 1982.
16. I. Gormeau, Numerical stability in Quasi-static Elasto/visco-plasticity, Internat. J. Numer, Meths. Eng. 9(19750 109-127.
17. G. E. Dieter, mechanical Metallurgy, 90, 3rd ed., McGraw-Hill(1986).
18. W. L. Dwight, A Thermal nad Stress Analysis of a Composite nuclear Fuel Rod using nunlinear Finite Element Techniques. University of Arkansas PhD thesis. (1982).
19. M. M. El.-Wakil, Nuclear Heat Transport, 253, International Textbook Compny (1971)
20. L. M. Kachanov, Foudations of the Theory of Placticity, 55, North-Holland Publishing Co. (19710.
21. S. P. Timoshenco and J. N. Goodier, Theory of Elasticity, 444, McGraw-Hill Co. (1970)
22. S. J. Ha Thermo-mechanical Analysis of a Cracked Fuel Pellet and cladding using the FEM, KAIST, Master Thesis, 1986.